Research Article Vol. 31, No. 18 / 28 Aug 2023 / Optics Express 29606
Optics EXPRESS

Compressed sensing framework for BCG signals based on the optical fiber sensor

SHUYANG CHEN,[1] HUAIJIAN LUO,[2] WEIMIN LYU,[2] JIANXUN YU,[3] JING QIN,[1,4] AND CHANGYUAN YU[2,*]

[1]Center of Smart Health, School of Nursing, The Hong Kong Polytechnic University, Hong Kong
[2]Photonics Research Institute, Department of Electronic and Information Engineering, The Hong Kong Polytechnic University, Hong Kong
[3]Department of Computer Science and Engineering, Chinese University of Hong Kong, Hong Kong
[4]harry.qin@polyu.edu.hk
[*]changyuan.yu@polyu.edu.hk

Abstract: A compressed sensing (CS) framework is built for ballistocardiography (BCG) signals, which contains two parts of an optical fiber sensor-based heart monitoring system with a CS module and an end-to-end deep learning-based reconstruction algorithm. The heart monitoring system collects BCG data, and then compresses and transmits the data through the CS module at the sensing end. The deep learning-based algorithm reconstructs compressed data at the received end. To evaluate results, three traditional CS reconstruction algorithms and a deep learning method are adopted as references to reconstruct the compressed BCG data with different compression ratios (CRs). Results show that our framework can reconstruct signals successfully when the CR grows from 50% to 95% and outperforms other methods at high CRs. The mean absolute error (MAE) of the estimated heartbeat rate (HR) is lower than 1 bpm when the CR is below 95%. The proposed CS framework for BCG signals can be integrated into the IoMT system, which has great potential in health care for both medical and home use.

1. Introduction

With the increasing aging of the population and the rapid progress of science and technology, intelligent healthcare has attracted extensive concern from people. Vital signs monitoring can assess the health condition of the body, which is significant in various healthcare applications. Among them, the heartbeat is one of the most important indicators of vital signs, since cardiovascular diseases (CVDs) have become the leading cause of death among various fatal diseases around the world [1]. There are various methods to monitor heartbeats, such as electrocardiography (ECG) and photoplethysmography (PPG), which can detect cardiac activities based on wearable devices [2,3]. However, contact measurement methods may cause skin allergy in daily-life cardiac monitoring. Ballistocardiography (BCG) is a measurement of body recoils produced by heart ejection during each cardiac cycle. The BCG waveform is generated with each cardiac contraction and owns several peaks and valleys. A completed BCG signal contains multiple peaks including H, I, J, K, and L peaks, and these peaks have corresponding physiological significance. For instance, the amplitude of the major wave J peak is related to the aortic pulse pressure [4]. Among them, the IJK complex is the combination of I, J, and K peaks on a BCG. It is the central and most visually obvious part of the typical BCG tracing, which can be used to calculate the heartbeat rate (HR) and heart rate variability (HRV) of the subject. BCG has great potential in cardiac health monitoring due to its non-invasive and non-contact measurement way.

Long-term, real-time, and remote services are essential for heartbeat monitoring whether in the clinic or at home. They can provide early detection of CVDs and avoid severe cardiovascular events. Benefiting from the development of information technology, vital signs sensors can be

#499746 https://doi.org/10.1364/OE.499746
Journal © 2023 Received 7 Jul 2023; revised 29 Jul 2023; accepted 2 Aug 2023; published 21 Aug 2023

Optics EXPRESS

integrated into the Internet of Things (IoT) systems to monitor physiological status, which is called the Internet of Medical Things (IoMT) systems [5]. The equipped sensors can monitor the vital signs such as heartbeat, breathing, and temperature from users continuously and transmit these data to cloud servers for further analysis. However, IoMT systems need to collect and store data at large data rates from abundant sensors. Thus, signal compression methods are necessary, which can reduce data size and ensure signal integrity. Compressed sensing (CS) is a signal sampling technique, which collects signals with fewer sampling rates and reconstructs signals by utilizing their intrinsic sparsity [6]. Traditional Shannon sampling theorem requires a higher sampling, resulting in larger data size, while CS overcomes this problem subjecting to certain conditions. Typically, the process of CS is that raw signals are collected and compressed simultaneously based on a well-designed measurement matrix and then transmitted to the cloud servers by the sensing end. Finally, compressed signals can be reconstructed at the receiving end. Compared to other compression methods, CS moves the computational load from sensors to the receiving end. The receiving end is typically located on cloud servers with great computational resources, where compressed signals can be reconstructed by algorithms with heavy computation, thus reducing the hardware complexity and saving energy at the sensing end. Benefiting from this, CS is widely used for data compression in IoT systems. Currently, there are many studies about using CS in physiological signals, such as ECG and PPG [7,8]. However, there are few studies about BCG signal compression based on CS. Therefore, we propose to develop a CS framework for BCG signal, which consists of an optical fiber sensor-based heart monitoring system at the sensing end, and a deep learning-based reconstruction algorithm at the received end.

The heart monitoring system at the sensing end can collect, compress and transmit the BCG data, which contains a BCG sensor and a CS module. For the BCG sensor, there are three common ways to obtain BCG signals, including weighing-scale-based, bed-based, and chair-based BCG sensors, corresponding to standing, lying, and sitting positions, respectively. Different types of sensors have been proposed to measure BCG signals during the last decade. For example, a standing BCG monitor modified by a commercial bathroom scale was proposed by Inan et al. [9]. The detected HRs in BCG signals were consistent with the results in the synchronized Doppler echocardiogram. For bed-based BCG sensors, numerous pressure-sensitive electrode sensor arrays have been designed in place of a single sensor to record BCG for sleeping monitoring by Kortelainen et al. [10]. In addition, Walter et al. monitored BCG using an EMFi sensor that was placed in the seat of the vehicle to track the fitness of the driver [11]. However, the electronic sensor-based BCG detection approaches have the inherent drawbacks of low sensitivity and being vulnerable to electromagnetic interference. In particular, optical fiber sensors, with the merits of low cost, lightweight, and being immune to electromagnetic interference have been widely applied in BCG detection. For example, micro-bend optical fiber sensors, fiber Bragg grating strain sensors, a wearable sensor based on stretchable elastomer optical fiber, and optical fiber interferometers are all investigated and successfully developed to measure BCG signals [12–15]. Here we adopt a high-sensitivity optical fiber interferometer to fabricate the BCG sensor. To process the BCG signals, a CS module built on a microcontroller unit (MCU) is placed at the end of the BCG sensor. The CS module can convert analog BCG signals into digital signals and compress them at the sensing end, and finally transmits them to the remote received end.

The deep learning-based algorithm at the received end is used to reconstruct the BCG signal. There are several traditional reconstruction algorithms in CS, such as greedy algorithms, convex optimization algorithms, and Bayesian learning algorithms [16]. The principles of the above reconstruction algorithms are to search for the optimal solution iteratively according to prior knowledge. Thus, these algorithms are time-consuming and require an assumption about the structure of signals, which are unsuitable for real-time monitoring. Recently, many deep learning models have been applied to reconstruct physiological signals, but rare research has been done

Optics EXPRESS

on BCG. There are some close works in spirit to ours, which are shown in the following. Gogna et al. proposed to adopt an autoencoder to reconstruct the biosignals including ECG and electroencephalography (EEG), in which the reconstruction results were proved to be superior to the commonly used BSBL-BO [17]. Zhang et al. developed a CSNet for ECG reconstruction, which contains a convolutional neural network (CNN) and a long short-term memory network (LSTM) [18]. The CNN is used to reconstruct the signal and the LSTM is adopted to denoise the recovered signals. However, these methods need to upsample the compressed signals in advance, and then map the rising-dimension signal to the original signal by the deep learning model. Therefore, we proposed an end-to-end deep learning model, which contains a fully connected layer (FCL) and U-net to reconstruct the compressed BCG signals, and we call it FCL + U-net. Among them, the FCL is used to rising the dimension of the compressed signal while the U-net is adopted to reconstruct the signal. Compared to the mentioned deep learning model, the compressed signal can be directly fed into the model without requiring the preprocessing step of upsampling.

In conclusion, we proposed a CS framework for BCG signals in this paper, which consists of two parts: an optical fiber sensor-based heart monitoring system with a CS module and an end-to-end deep learning-based reconstruction algorithm. The heart monitoring system can collect and compress the BCGs and transmit them to the cloud server at the sensing end. Then, the proposed algorithm can reconstruct the BCG signal at the received end. To evaluate the performance of our framework, several commonly used CS reconstruction methods in ECG, including basis pursuit (BP), orthogonal matching pursuit (OMP), bound-optimization-based block sparse Bayesian learning (BSBL-BO), and deep learning method are adopted as references. The proposed method outperforms other methods at high compression ratios (CRs). In addition, the mean absolute error (MAE) of the estimated heartbeat rate (HR) is lower than 1 bpm when the CR is below 95%. To our knowledge, it is the first time to develop a CS framework including the sensing system, the compressed module, and the reconstruction algorithm for BCG signals. The optical fiber sensor-based heart monitoring system with CS framework can be integrated into the IoMT system, which has great potential in daily cardiac monitoring.

2. CS framework

2.1. Principle

CS is a novel signal acquisition technique, and it can collect signals using a sampling rate far below the Nyquist sampling frequency and then reconstruct signals based on the sparsity. A basic model can be given as

$$\boldsymbol{y} = \boldsymbol{\Phi x}, \tag{1}$$

where $\boldsymbol{x} \in \mathbb{R}^{N\times 1}$ is the original signal and its dimension is N, and $\boldsymbol{\Phi} \in \mathbb{R}^{M\times N}$ ($M \ll N$) is the measurement matrix, which is designed to linearly compress x. In the $\boldsymbol{\Phi}$, any M columns are linearly independent. In our case, $\boldsymbol{x}$ is a segment of obtained BCG signals from the optical fiber sensor. $\boldsymbol{y}$ is the M-dimension compressed signal produced by the CS module at the sensing end and then transmitted to the receiving end.

For many measurements, most natural signals are not sparse in practice. The signal can be transformed into the sparse domain by the transform algorithms, such as Fourier transform and wavelet transform. Therefore, $\boldsymbol{x}$ can be described as $\boldsymbol{x} = \boldsymbol{\Psi\theta}$, where $\boldsymbol{\Psi} \in \mathbb{R}^{N\times N}$ is an orthonormal basis matrix of the selected transformed domain, and $\boldsymbol{\theta}$ is a sparse vector with N dimension. Thus, Eq. (1) can be rewritten as

$$\boldsymbol{y} = \boldsymbol{\Phi\Psi\theta} = \boldsymbol{\Omega\theta}, \tag{2}$$

where $\boldsymbol{\Omega} \triangleq \boldsymbol{\Phi\Psi}$ is called the sensing matrix. As mentioned above, $\boldsymbol{\theta}$ is a sparse vector, and thus the CS algorithm can reconstruct $\boldsymbol{\theta}$ based on the $\boldsymbol{y}$ and $\boldsymbol{\Omega}$. Since Eq. (2) is an underdetermined

Optics EXPRESS

equation, it has infinitely many solutions. Among all the solutions, the sparsest solution is the desired reconstructed signal. Therefore, the problem of solving the equation $\boldsymbol{y} = \boldsymbol{\Phi x}$ can be transformed into the minimum 0-norm problem:

$$min||\boldsymbol{\theta}_0|| \qquad \text{subject to} \qquad \boldsymbol{\Omega\theta} = \boldsymbol{\Phi\Psi\theta} = \boldsymbol{y}. \tag{3}$$

The signal reconstruction algorithm is to use the M-dimension measurement signal $\boldsymbol{y}$ and measurement matrix $\boldsymbol{\Phi}$ to reconstruct the N-dimension original signal $\boldsymbol{x}$. The signal reconstruction issue in the CS is equivalent to the sparse decomposition problem, so the existing algorithms of sparse decomposition have been applied to the CS signal reconstruction, such as convex optimization algorithms, greedy algorithms, and Bayesian learning algorithms. Among them, BP is one of the most common convex optimization algorithms. It converts the L_0 norm problem into a simpler L_1 norm minimum optimization problem so that the linear programming method can be used to solve it [19]. Greedy algorithms, such as matching pursuit (MP) and orthogonal matching pursuit (OMP), solve the problem by selecting the locally optimal choice at each stage [20]. BSBL-BO is a reconstruction algorithm based on the Bayesian learning algorithm, which solves the problem by utilizing the spatial structure and temporal structure of the solution [21]. However, these solutions are iterative and thus time-consuming, which cannot be applied in real-time monitoring. Therefore, the deep learning model is proposed to reconstruct the compressed signal. The basic idea is that Φ^T is multiplied on both sides of Eq. (1), and we can obtain

$$\boldsymbol{x'} = \boldsymbol{\Phi^T y} = \boldsymbol{\Phi^T \Phi x}, \tag{4}$$

where $\boldsymbol{x'}$ can be considered as a noisy version of the original signal $\boldsymbol{x}$. The deep learning model, such as autoencoder [17], can be used to learn the mapping between the noisy signal $\boldsymbol{x'}$ and the original signal $\boldsymbol{x}$. The task can be described as $\hat{\boldsymbol{x}} = f(\boldsymbol{x'})$, where $\hat{\boldsymbol{x}}$ is the reconstruction signal and the f is the mapping model. The reconstruction process is divided into two steps. First, $\boldsymbol{y}$ is risen from M dimension into N dimension by multiplying $\boldsymbol{\Phi^T}$, and then the deep learning model is trained to map from a noisy input $\boldsymbol{x'}$ to a clear output $\hat{\boldsymbol{x}}$. To simplify the reconstruction process, we use an FCL to replace the first step to raise the dimension of $\boldsymbol{y}$, and thus the proposed model can build a mapping from the compressed input $\boldsymbol{y}$ to the clean output $\hat{\boldsymbol{x}}$ directly, which is $\hat{\boldsymbol{x}} = f(\boldsymbol{y})$.

To build a CS framework for BCG signals, our works include two parts. The first one is the heart monitoring system, which can collect, compress and transmit the data at the sensing end. The second one is a deep learning-based CS reconstruction algorithm at the received end to recover the BCG signal. Detailed information on these two parts is given in the following sections.

2.2. Optical fiber sensor-based heart monitoring system with CS module

Our chair-based heart monitoring system is made up of a BCG sensor and a CS module, as shown in Fig. 1. Among them, the BCG sensor is fabricated by an optical fiber Mach-Zehnder interferometer (MZI), a phase-sensitive optical fiber sensor. When the subject sits on the chair with the BCG sensor, the body recoils derived from heartbeats can cause a phase difference in the MZI. Then the intensity varying with the phase difference can be detected by a photodetector (PD), which is the BCG signal. The CS module is built on an MCU, and it contains the measurement matrix which can compress BCG signals according to the CS method. When the CS module receives a raw BCG signal, it can compress and transmit the signal to cloud servers. The details of the BCG sensor and the CS module are given as follows.

The detail of the BCG sensor is shown in Fig. 1(a), which contains a low-cost optical source (distributed-feedback laser operating at 1550 nm), an MZI, and a low-speed PD. In the MZI, two 3 dB couplers respectively work as the optical splitter and the optical coupler to create

Optics EXPRESS

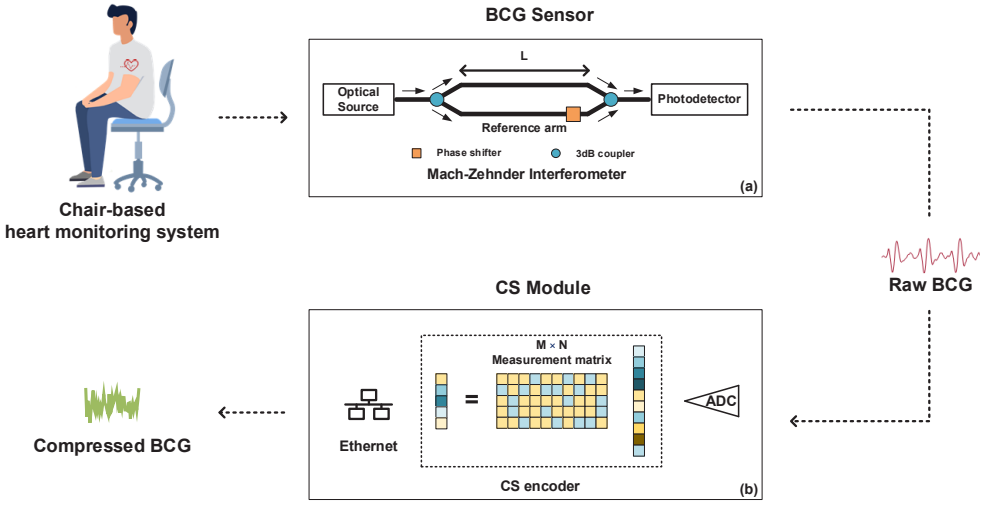

Fig. 1. The heart monitoring system.

interference. The interference light intensity I can be described as

$$I = I_s + I_r + 2\sqrt{I_s I_r}\cos(\varphi), \tag{5}$$

where I_s and I_r are light intensities from the sensing and reference arms, respectively. φ is the phase difference within two arms introduced by body recoils caused by heartbeat, and it can be expressed by

$$\varphi = \frac{2\pi n}{\lambda}(L_s - L_r) = \frac{2\pi n}{\lambda}\delta L, \tag{6}$$

where n represents the refractive index of the single-mode fiber in the MZI while λ is the central wavelength of the optical source. L_s and L_r are lengths of sensing and reference arms, and their length difference is denoted as δL. The sensing and reference arms of MZI are placed parallelly on a plastic substrate that can be packaged as a smart cushion to monitor BCG in a non-invasive way. To make the sensor better embedded into a cushion, the parameters of 40/40.5 cm and 5 mm are chosen as lengths of two arms and the length difference between them. Since the environmental noise can introduce phase drift in the MZI and further cause the signal fading problem, we use the phase compensation system to overcome this issue. The phase compensation system adopts a low-cost phase shifter and a proportional-integral-derivative (PID) controller to adjust the operating point. The phase shifter is fixed with the reference arm outside the sensing area, and it can cause a very slight phase difference in the MZI. The PID controller calculates the operating point drift in the MZI produced by the phase drift owing to the environment noise, and then controls the phase shifter to compensate for the phase drift. In this way, the output of the MZI can be kept in quadrature and the signal fading problem is addressed. Compared to traditional phase modulation methods, this scheme owns the merits of low cost and easy integration.

The structure of the CS module is shown in Fig. 1(b), which is developed on a low-cost MCU (ARM microcontroller STM32F107). The module is a portable IOT device and it integrates several functions including data acquisition, CS encoder, and transmission. When the electrical signal from the BCG sensor feeds into the CS module, the analog-digital converter (ADC) can sample analog signals into digital signals with 12-bit resolution. The digital data is stored in the register, and each time when the sampling point reaches the array length N, the register will feed these data into the CS encoder. The CS encoder stores an $M \times N$ measurement matrix, where M

Optics EXPRESS

is the length of compressed data and it the much less than N depending on the CR. We use the sparse random matrix as the measurement matrix, where L elements in each column are selected randomly to set as 1, and the remaining $M-L$ elements are set as 0. Through the CS encoder, the N dimension digital signal can be compressed into an M dimension digital signal. During the process of matrix calculation in the MCU, each unit is represented by 3 bytes (24-bit) to avoid overflow. Finally, the data is normalized into 16-bit resolution and sent to the cloud server by Ethernet (DM9161A) through MQTT protocol. Several parameters such as the size of the measurement matrix and sampling rate are chosen taking into account the running speed and memory of the MCU, as well as the structure of the follow-up deep learning-based reconstruction algorithm. In the experiment, the sampling rate of the ADC collection is 250 Hz, and the length stored in the register, N, is set to 512. In addition, we evaluate the performance of this framework based on different CRs (50% to 96%), and thus M varies from 256 to 20.

2.3. Deep learning-based CS reconstruction algorithm

At the receiving end, we propose a deep learning-based algorithm to reconstruct the BCG signals. The workflow of building the reconstruction algorithm is shown in Fig. 2. The original BCG is compressed by the measurement matrix, in which a proportion of compressed data are selected as training data and used to train the network. The optimization parameters in the network will be saved during training, and then the model can be used to reconstruct the compressed BCG signals.

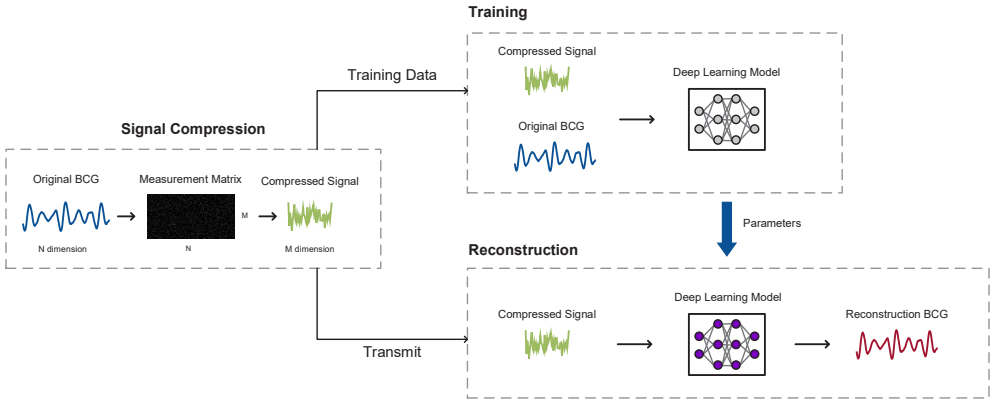

Fig. 2. The workflow of building the reconstruction algorithm based on a deep learning model.

The architecture of the deep learning model, FCL + U-net, is shown in Fig. 3. It is an end-to-end model, and thus the compressed signals $\boldsymbol{y}$ can be directly fed into the model. The model consists of an FCL and a modified U-net network. The FCL is used to map the compressed signal $\boldsymbol{y}$ from M dimension to N dimension. The activation function of FCL is tanh, which outputs the value from -1 to 1. It can speed up the following training process and improve the accuracy of the model. The feature map with the size of $N \times 1$ is then fed into a modified U-net, which is used to reconstruct the BCG signals. Similar to the typical structure of the U-net [22], the modified U-net consists of encoding and decoding parts. In the encoding stage, each encoder contains two 1-D convolutional layers followed by a max pooling layer to halve the size of feature maps. The number of filter channels n_f is twice as many as the previous block. During the decoding step, an upsampling layer followed by a convolutional layer in the decoder block is used to double the size of the feature map and cut the number of feature channels in half. The feature map in the symmetric encoding block is integrated with the upsampled feature map in the decoding block. The combined feature map is then fed into two 1-D convolutional layers. The number of

Optics EXPRESS

filter channels n_f is halved in each decoder. Finally, a convolutional layer with a linear activation function is used as the output layer to reconstruct the BCG waveform.

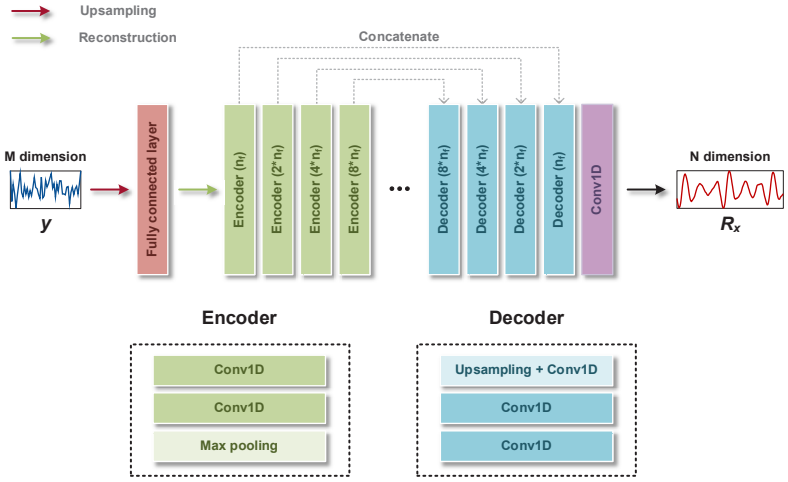

Fig. 3. The architecture of the end-to-end deep learning model.

2.4. Evaluation methods

In this experience, we adopt three metrics to estimate the reconstruction results, including percent root mean square difference (PRD), Pearson correlation coefficient (PCC), and mean square error (MSE) [23]. Among them, PRD represents the error between reconstructed and original signals, and a smaller PRD is desirable, which represents the higher performance of the reconstruction algorithm. Three metrics are described in Eq. (7)-(9) respectively, where R_x and x are reconstructed and original BCG signals.

$$\mathrm{PRD}\,(\%) = \sqrt{\frac{\sum_{n=1}^{N}(R_x(n)-x(n))^2}{\sum_{n=1}^{N}(x(n))^2}} \times 100, \tag{7}$$

$$\mathrm{PCC} = \frac{\sum_{n=1}^{N}(R_x(n)-\overline{R_x})(x(n)-\bar{x})}{\sqrt{\sum_{n=1}^{N}(R_x(n)-\overline{R_x})^2}\sqrt{\sum_{n=1}^{N}(x(n)-\bar{x})^2}}, \tag{8}$$

$$\mathrm{MSE} = \frac{1}{N}\sum_{n=1}^{N}(R_x(n)-x(n))^2. \tag{9}$$

In addition, IJK complex containing I, J, and K peaks is the most important part of BCG compared with other peaks, since the J-J interval can be used to calculate the HR and HRV. The IJK complex and J-J interval are shown in Fig. 4. Therefore, to evaluate the reconstruction result of IJK complex, we calculate HRs based on reconstruction BCG signals and compare the results with reference HRs obtained from raw BCG signals.

CR is a measurement of the relative reduction in data size after signal compression and it can be defined as

$$CR = \frac{N-M}{N} \times 100,$$

where N and M are the length of the original signal and the compressed signal. In the CS framework, the CR is adjusted by changing the shape of the measurement matrix in the CS

Optics EXPRESS

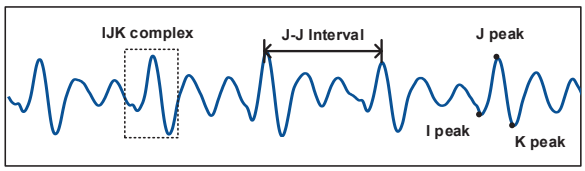

Fig. 4. A segment of BCG.

module. As mentioned, the measurement matrix is a two-dimensional matrix with the size of $M \times N$. To explore the reconstruction results with different CRs, N is fixed at 512 and M declines from 256 to 20, of which the corresponding CR is from 50% to 96%. The workflow of the evaluation method is shown in Fig. 5. Firstly, the measurement matrices are designed into different sizes, and the compressed signals with different CRs can be obtained. Secondly, the data are divided into training, validation, and test set. The training and validation data are used to train and optimize the deep learning model, and the test set is used to verify the reconstruction results using different algorithms, including traditional reconstruction algorithms and deep learning models. The model is trained separately for each CR. Finally, four metrics including PRD, PCC, MSE, and HR are adopted to evaluate the reconstruction results in the test set.

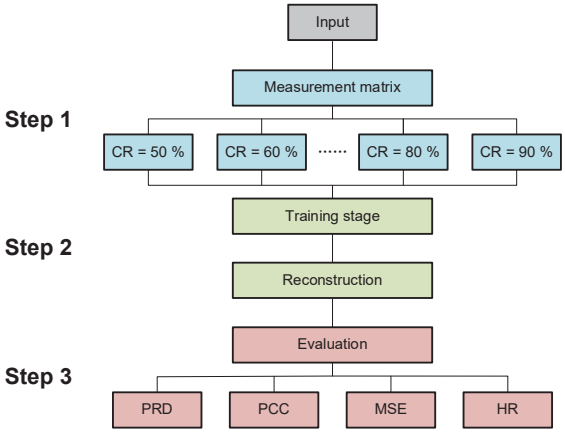

Fig. 5. The workflow of the evaluation method.

3. Results and discussions

In this experiment, we have 14370 BCG segments collected from our heart monitoring system, in which each segment owns 512 sampling points. The ratio between the training, validation, and test sets is 6, 2, and 2. We have conducted a series of experiments to optimize the parameters in the deep learning model. Adam optimization method [24] with default parameters (learning rate: 0.001, beta-1: 0.9, beta-2: 0.99) is used as the optimizer. MSE is chosen as the loss function and mini-batch gradient descent is adopted, in which the batch size is 16. The kernel size of filters is 25×1, and the number of filters (n_f) is 64, which doubles at each encoding stage while halves at each decoding stage.

Reconstruction results from the deep learning models and traditional reconstruction algorithms with the CR ranging from 50% to 90% are presented first. Since there are few works about the CS framework for BCG signals, we select several traditional reconstruction algorithms performing well on the ECG as references to explore the performance of traditional algorithms of CS for BCG

Optics EXPRESS

signal reconstruction. Three commonly used reconstruction algorithms are chosen, which are BP, OMP, and BSBL-BO. In addition, two deep learning models are adopted in the experiment. One is our proposed end-to-end FCL + U-net, which develops the mapping from $\boldsymbol{y}$ to $\boldsymbol{x}$ directly. The other one is a U-net, which builds the mapping from $\boldsymbol{x}'$ to $\boldsymbol{x}$, where $\boldsymbol{x}'$ is obtained by Eq. (4). We use 2874 BCG segments in the test set to compare the performance of deep learning models and traditional algorithms. The average PRD, PCC, and MSE of results recovered by five types of reconstruction algorithms under different CRs are shown in Fig. 6(a), (b), and (c). On the whole, FCL + U-net and BSBL-BO outperform BP, OMP, and U-net. BP and OMP present acceptable results when the CR is low than 70% while their performances are poor beyond that. U-net is not sensitive to the change of CR in this range. For PRD, the performance of BSBL-BO is slightly better than that of FCL + U-net when the CR is below 80%. For PCC and MSE, the performances of BSBL-BO and FCL + U-net are both good with the CR below 80%. It can be found that all indicators of FCL + U-net are better than BSBL-BO when the CR exceeds 80%. In general, FCL + U-net can give satisfying results with the CR ranging from 50% to 90%. However, we find that with the increasing CR, the performance of BSBL-BO declines noticeably. The reconstruction waveforms of a BCG segment with 94% CR using BSBL-BO, U-net, and FCL + U-net are shown in Fig. 7(a), (b), and (c), where the red line is reconstruction BCG and the blue line is the original signal. For the high CR, BSBL-BO fails to reconstruct the BCG waveform, in which one peak in the dotted box is incorrectly recovered as the IJK complex. Interestingly, U-net can operate with a high CR though it performs worse than the traditional algorithms when the CR is low than 70%. It can be found that the performances of FCL + U-net are still good when the CR exceeds 90%, and thus we continue to increase the CR to explore the limits of the deep learning model.

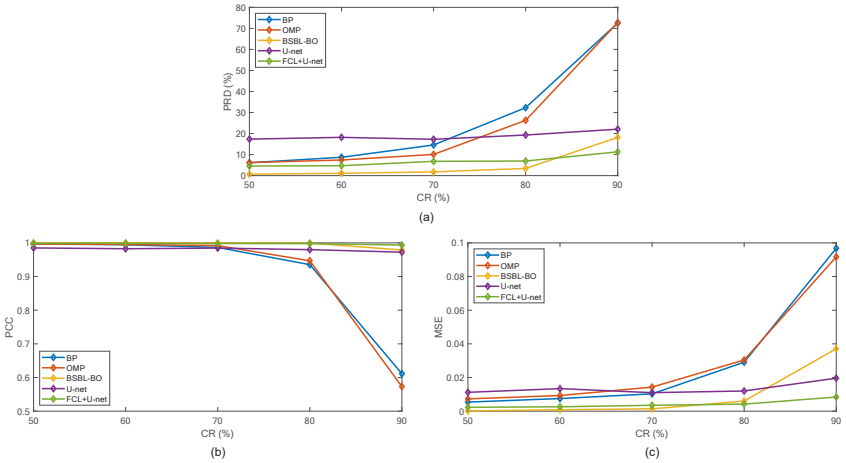

Fig. 6. The average (a) PRD, (b) PCC, and (c) MSE in the test set recovered by five types of reconstruction algorithms with the CR ranging from 50% to 90%.

We compress the BCG segments using the measurement matrices with high CRs from 91% to 96%, and the training and evaluation scheme is the same as before. The average PRD, PCC, and MSE of reconstruction results in the test set using two deep learning models, U-net and FCL + U-net with the CR exceeding 90% are shown in Table 1. Since the performances of traditional reconstruction algorithms including BP, OMP, and BSBL-BP are poor with a high CR and thus these algorithms are not adopted for comparison. It can be found that FCL + U-net still outperforms U-net in high CRs for three indicators. With the increasing CR, the performance of FCL + U-net decreases gradually and its results become poor when the CR reaches 96%. The reconstructive BCG waveforms using FCL + U-net with CR from 91% to 96% are shown in

Optics EXPRESS

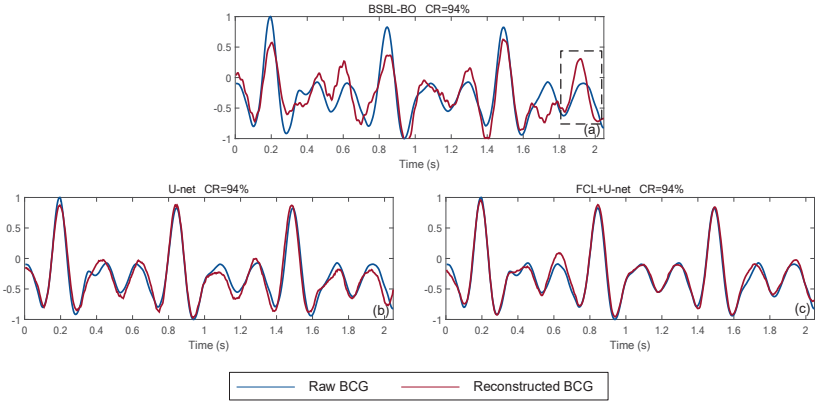

Fig. 7. Reconstruction results by (a) BSBL-BO, (b) U-net and (c) FCL + U-net with 94% CR.

Fig. 8(a) to (f). From these figures, we can find that though performance decline with the increase of CR, the IJK complex in the BCG can still be recovered. The performance degradations mainly result from the not-so-good recovery of other less important peaks on the BCG. It is quite different from the other cases based on traditional algorithms, in which the reconstructions are poor for both the IJK complex and the non-IJK complex with the high CRs.

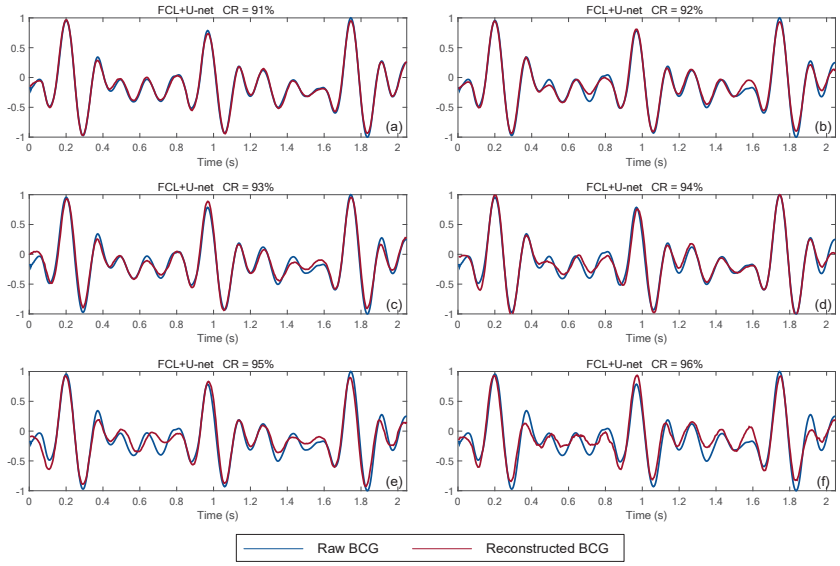

Fig. 8. Reconstruction waveform based on FCL + U-net with different CRs including (a) 91%, (b) 92%, (c) 93%, (d) 94%, (e) 95%, and (f) 96%.

To evaluate the reconstruction results of the IJK complex, HRs are estimated based on the reconstruction signals in the test set. We compare the estimated HRs based on two groups of BCG signals reconstructed by U-net and FCL + U-net, respectively. Reference HRs are calculated by the original signals. The scatterplots of estimated HRs versus reference HRs are shown in Fig. 9. Among them, Fig. 9(a) to (c) are the estimated results based on U-net with the CR ranging from 93% to 95% while Fig. 9(d) to (f) are related to estimated results from FCL + U-net. The HR ranges from 60 bpm to 110 bpm in the test set. It can be found that FCL + U-net outperforms

Optics EXPRESS

Table 1. The average PRD, PCC, and MSE of the reconstruction results in the test set based on the deep learning models with high CRs.

CR	PRD		PCC		MSE	
	FCL + U-net	U-net	FCL + U-net	U-net	FCL + U-net	U-net
91%	12.864	27.582	0.992	0.957	0.011	0.025
92%	16.758	30.147	0.985	0.948	0.010	0.023
93%	20.100	30.419	0.978	0.947	0.016	0.022
94%	25.539	33.419	0.964	0.935	0.026	0.033
95%	28.082	36.261	0.955	0.925	0.028	0.036
96%	34.780	44.410	0.929	0.881	0.030	0.042

U-net in the task of HR estimation. The PCC between the estimated HRs and reference HRs are 0.998, 0.961, and 0.943 with CRs from 93% to 95%, which is much higher than that of U-net (0.934, 0.881, and 0.769). MAE of estimated HRs in the test data with CR increasing from 91% to 96% based on U-net and FCL + U-net are shown in Fig. 10. It can be found that with the CR below 95%, MAE of estimated HRs is less than 1 bpm based on FCL + U-net while MAE exceeds 1 bpm when CR reaches 94% for U-net. To balance the accuracy of signal reconstruction and data transmission load, we can use the compressed signal with a CR below 95% for the data transmission.

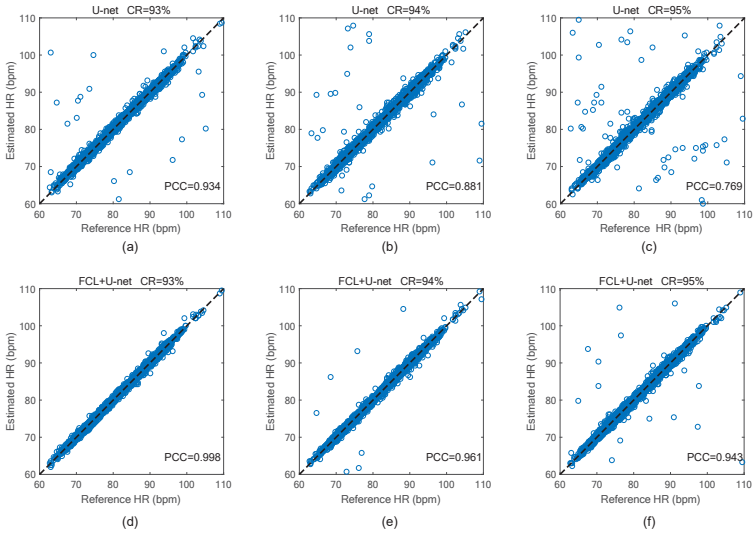

Fig. 9. Scatterplots of estimated HRs in reconstruction signals versus reference HRs based on: (a) U-net with 93% CR, (b) U-net with 94% CR, (c) U-net with 95% CR, (d) FCL + U-net with 93% CR, (e) FCL + U-net with 94% CR, and (f) FCL + U-net with 95% CR.

Through the experiment, we can find that the deep learning models outperform traditional algorithms in the high CR. In addition, they are dozens of times fast than the traditional reconstruction algorithms, which is more suitable for a real-time monitoring system. Comparing the two deep learning models, FCL + U-net performs well than U-net according to three metrics including PRD, PCC, and MSE, and also the HR estimation. We think the main reason is that for U-net, $\boldsymbol{\Phi}^{\boldsymbol{T}}$ is used to raise the dimension of the compressed signal $\boldsymbol{y}$, and thus $\boldsymbol{x}'$ is fixed. However, for FCL + U-net, the dimension of $\boldsymbol{y}$ is risen by the FCL, and the parameters of it can be optimized through training. In this work, we use MSE as the loss function to train the neural

Optics EXPRESS

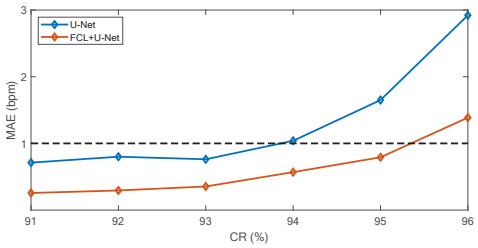

Fig. 10. MAE of estimated HRs based on U-net and FCL + U-net with the CRs ranging from 91% to 96%.

network, and thus the model tends to optimize the parameters only depending on this metric. To further improve the result, we will attempt to design a combinative loss function to train the deep learning model.

4. Conclusion

In this paper, we propose a CS framework for BCG signals. The framework consists of two parts of an optical fiber sensor-based heart monitoring system with a CS module and an end-to-end deep learning-based reconstruction algorithm. BCG signals can be obtained, compressed, and transmitted by the heart monitoring system athe sensing end. Then, the proposed reconstruction algorithm can recover the signal at the received end. To evaluate the performance of our farmwork, we compare the results with three traditional CS reconstruction algorithms, BP, OMP, and BSBL-BO, and a deep learning method. The results show that our system can reconstruct signals well when the CR is lower than 95%, in which the MAE of the estimated HRs is lower than 1 bpm. The proposed CS framework for BCG signals can be integrated into the IoMT system, which can provide daily cardiac health monitoring for both medical and home use.

Funding. Shenzhen-HK-Macao Science and Technology Plan C (Grant SGDX2020110309520303); University Grants Committee (Grant 15200718); National Natural Science Foundation of China (61971372).

Disclosures. The authors declare no conflicts of interest.

Data availability. Data underlying the results presented in this paper are not publicly available at this time but may be obtained from the authors upon reasonable request.

References

1. K. M. Namara, H. Alzubaidi, and J. K. Jackson, "Cardiovascular Disease as a Leading Cause of Death: How Are Pharmacists Getting Involved?" Integr. Pharm. Res. Pract. **8**, 1–11 (2019).
2. P. Kligfield, L. S. Gettes, J. J. Bailey, R. Childers, B. J. Deal, E. W. Hancock, G. V. Herpen, J. A. Kors, P. Macfarlane, D. M. Mirvis, O. Pahlm, P. Rautaharju, and G. S. Wagner, "Recommendations for the standardization and interpretation of the electrocardiogram: part I: the electrocardiogram and its technology a scientific statement from the American Heart Association Electrocardiography and Arrhythmias Committee, Council on Clinical Cardiology; the American College of Cardiology Foundation; and the Heart Rhythm Society endorsed by the International Society for Computerized Electrocardiology," J. Am. Coll. Cardiol. **49**(10), 1109–1127 (2007).
3. S. A. Mascaro and H. H. Asada, "Photoplethysmograph fingernail sensors for measuring finger forces without haptic obstruction," IEEE Trans. Robot. Autom. **17**(5), 698–708 (2001).
4. C. S. Kim, S. L. Ober, M. S. Mcmurtry, B. A. Finegan, O. T. Inan, R. Mukkamala, and J. O. Hahn, "Ballistocardiogram: Mechanism and Potential for Unobtrusive Cardiovascular Health Monitoring," Sci. Rep. **6**(1), 31297 (2016).
5. G. J. Joyia, R. M. Liaqat, A. Farooq, and S. Rehman, "Internet of medical things (IoMT): Applications, benefits and future challenges in healthcare domain," J. Commun. **12**(4), 240–247 (2017).
6. D. L. Donoho, "Compressed sensing," IEEE Trans. Inf. Theory **52**(4), 1289–1306 (2006).
7. J. Xiao, F. Hu, Q. Shao, and S. Li, "A low-complexity compressed sensing reconstruction method for heart signal biometric recognition," Sensors **19**(23), 5330 (2019).
8. G. D. Poian, B. Riccardo, and R. Rinaldo, "Separation and analysis of fetal-ECG signals from compressed sensed abdominal ECG recordings," IEEE. Trans. Biomed. Eng. **63**(6), 1269–1279 (2015).
9. O. T. Inan, M. Etemadi, R. M. Wiard, L. Giovangrandi, and G. T. A. Kovacs, "Robust ballistocardiogram acquisition for home monitoring," Physiol. Meas. **30**(2), 169–185 (2009).

Optics EXPRESS

10. J. M. Kortelainen and J. Virkkala, "FFT averaging of multichannel BCG signals from bed mattress sensor to improve estimation of heart beat interval," in *2007 29th annual international conference of the IEEE engineering in medicine and biology society*, 6685–6688 (2007).
11. M. Walter, B. Eilebrecht, T. Wartzek, and S. Leonhardt, "The smart car seat: Personalized monitoring of vital signs in automotive applications," Pers Ubiquit. Comput. **15**(7), 707–715 (2011).
12. X. Yang, Z. Chen, C. S. M. Elvin, L. H. Y. Janice, S. H. Ng, J. T. Teo, and R. Wu, "Textile Fiber Optic Microbend Sensor Used for Heartbeat and Respiration Monitoring," IEEE Sens. J. **15**(2), 757–761 (2015).
13. Ł. Dziuda, M. Krej, and F. W. Skibniewski, "Fiber Bragg grating strain sensor incorporated to monitor patient vital signs during MRI," IEEE Sens. J. **13**(12), 4986–4991 (2013).
14. B. Zha, Z. Wang, L. Li, X. Hu, B. Ortega, X. Li, and R. Min, "Wearable cardiorespiratory monitoring with stretchable elastomer optical fiber," Biomed. Opt. Express **14**(5), 2260–2275 (2023).
15. F. Tan, S. Chen, W. Lyu, Z. Liu, C. Yu, C. Lu, and H. Y. Tam, "Non-invasive human vital signs monitoring based on twin-core optical fiber sensors," Biomed. Opt. Express **10**(11), 5940–5952 (2019).
16. E. C. Marques, N. Maciel, L. Naviner, H. Cai, and J. Yang, "A review of sparse recovery algorithms," IEEE Access **7**, 1300–1322 (2018).
17. A. Gogna, A. Majumdar, and R. Ward, "Semi-supervised stacked label consistent autoencoder for reconstruction and analysis of biomedical signals," IEEE Trans. Biomed. Eng. **64**(9), 2196–2205 (2016).
18. H. Zhang, Z. Dong, Z. Wang, L. Guo, and Z. Wang, "CSNet: A deep learning approach for ECG compressed sensing," Biomed. Signal Process Control **70**, 103065 (2021).
19. R. Liu, M. Shu, and C. Chen, "ECG signal denoising and reconstruction based on basis pursuit," Appl. Sci. **11**(4), 1591 (2021).
20. J. A. Tropp and A. C. Gilbert, "Signal recovery from random measurements via orthogonal matching pursuit," IEEE Trans. Inf. Theory **53**(12), 4655–4666 (2007).
21. Z. Zhang, T. P. Jung, S. Makeig, and B. D. Rao, "Compressed sensing for energy-efficient wireless telemonitoring of noninvasive fetal ECG via block sparse Bayesian learning," IEEE. Trans. Biomed. Eng. **60**(2), 300–309 (2012).
22. O. Ronneberger, P. Fischer, and T. Brox, "U-Net: Convolutional Networks for Biomedical Image Segmentation," In *International Conference on Medical image computing and computer-assisted intervention*, 234–241 (2015).
23. K. Ranjeet, A. Kumar, and R. K. Pandey, "ECG signal compression using different techniques," in *International Conference on Advances in Computing, Communication and Control*, 231–241 (2011).
24. D. P. Kingma and J. Ba, "Adam: A method for stochastic optimization," arXiv, arXiv:1412.6980 (2014).